J Mater Sci (2010) 45:1782–1789
DOI 10.1007/s10853-009-4155-7

Material characterization of SS 316 in low-cycle fatigue loading

A. Dutta · S. Dhar · S. K. Acharyya

Received: 28 May 2009 / Accepted: 19 December 2009 / Published online: 20 January 2010

Abstract This study deals with simulation of low-cycle fatigue (LCF), followed by evaluation of fatigue parameters, which would be suitable for estimating fatigue lives under uniaxial loading. The cyclic elastic–plastic stress–strain responses were analyzed using the incremental plasticity procedures. Finite-element (FE) simulation in elastic–plastic regime was carried out in FE package ABAQUS. Emphasis has been laid on calibration of SS 316 stainless steel for LCF behavior. For experimental verifications, a series of low-cycle fatigue tests were conducted using smooth, cylindrical specimens under strain-controlled, fully reversed condition in INSTRON UTM (Universal Testing Machine) with 8,800 controller at room temperature. The comparisons between numerical simulations and experimental observations reveal the matching to be satisfactory in engineering sense. Based on the cyclic elastic–plastic stress–strain response, both from experiments and simulation, loop areas, computed for various strain amplitude, have been identified as fatigue damage parameter. Fatigue strain life curves are generated for fatigue life prediction using Coffin–Manson relation, Smith–Watson–Topper model, and plastic energy dissipated per cycle (loop area). Life prediction for LCF has been found out to be almost identical for all these three criteria and correlations between predicted and experimental results are shown. It is concluded that the improvement of fatigue life prediction depends not only on the fatigue damage models, but also on the accurate evaluations of the cyclic elastic–plastic stress/strain responses.

A. Dutta · S. Dhar · S. K. Acharyya (✉)
Department of Mechanical Engineering, Jadavpur University, Kolkata 700032, India
e-mail: skacharyya@mech.jdvu.ac.in

List of symbols

σ	Stress at any instant of time
ε	Strain at any instant of time
$\sigma_{\min}$	Minimum stress in a repeated stress cycle
$\sigma_{\max}$	Maximum stress in a repeated stress cycle
σ_{m}	Mean stress
σ_{y}	Yield stress
$\Delta\sigma$	Total stress range
$\Delta\varepsilon$	Total strain range
$\Delta\varepsilon_{\mathrm{e}}$	Total elastic strain range (elastic strain component)
$\Delta\varepsilon_{\mathrm{p}}$	Total plastic strain range (plastic strain component)
$N\ (or,\ N_{\mathrm{f}})$	Number of cycles to failure
$\sigma_{\mathrm{f}}\ (or, \sigma'_{\mathrm{f}})$	Fatigue strength coefficient
b	Fatigue strength exponent
$\varepsilon_{\mathrm{f}}\ (or, \varepsilon'_{\mathrm{f}})$	Fatigue ductility coefficient
c (or, m)	Fatigue ductility exponent
n'	Cyclic strain hardening exponent
K	Cyclic strength coefficient
$\sigma_1,\ \sigma_2,\ \sigma_3$	Principal stresses
Y	Yield stress in tension
f	Yield function
σ_{ij}	Stress tensor
S_{ij}	Deviatoric component of stress tensor σ_{ij}
α_{ij}	Back stress tensor
ε^{p}_{ij}	Plastic strain tensor
$\sigma_0,\ \sigma_c,\ \sigma_{yc}$	Current yield stress
$\varepsilon^{\mathrm{p}}_{\mathrm{eq}}$	Equivalent plastic strain
$R\left(\varepsilon^{\mathrm{p}}_{\mathrm{eq}}\right)$	Isotropic hardening function (a function of $\varepsilon^{\mathrm{p}}_{\mathrm{eq}}$)
b	A material constant (determines the rate of change of size of the yield surface with $\varepsilon^{\mathrm{p}}_{\mathrm{eq}}$)

Q (*or*, Q_∞)	A material constant (representative of the maximum change in size of the yield surface)
C	Initial kinematic hardening modulus
γ	Dynamic recovery term associated with non-linear kinematic hardening
H	Plastic hardening modulus
$\dot{\varepsilon}^{p}_{eq}$	Equivalent plastic strain rate
E_{ijkl}	Fourth-order elastic modulus tensor
D_{ijkl}	Fourth-order elasto-plastic modulus tensor
v	Poisson's ratio
σ_{max} (*or*, σ_{peak})	Maximum tensile stress
$\sigma_{a,rev}$	Fully reversed stress amplitude
$\varepsilon_{a,rev}$	Fully reversed strain amplitude
W_f	Total plastic strain energy dissipated prior to failure
ΔW	Average plastic strain energy dissipated per cycle

Introduction

SS 316 stainless steel is considered as the second most common grade of steel in stainless steel family after SS 304. Alloy addition of molybdenum prevents specific forms of corrosion. It is also known as marine grade stainless steel due to its increased resistance to chloride corrosion in comparison to type 304, and thus commonly finds usage in the building of nuclear reprocessing plants.

For major reactor structures, SS 316 has been considered as the most preferred material. Lower allowable strength of this material is acceptable. In order to compensate for lower carbon level, the maintenance of strength is ensured by addition of nitrogen up to a maximum of 0.12% [1]. In view of proposed design of 100 years from Advanced Heavy Water Reactor (AWHR), SS 316 has been identified as a preferred choice, compared to other grades of stainless steel, in terms of its response to satisfy the general structural integrity concerns such as fatigue, fracture, general erosion, and corrosion [2]. Thus, SS 316 can be considered as an important material in the construction of nuclear power plant components.

Wong et al. [3] investigated low- and high-cycle fatigue in 316 stainless steel, where they subjected the specimens to varying degrees of LCF and then to high-cycle fatigue (HCF) till fracture. Fatigue tests were carried out under strain-controlled loading conditions, where two strain amplitudes in the LCF range with a common HCF strain amplitude were investigated. Results showed that fatigue life decreased when specimens were introduced to increasing numbers of initial LCF. Thus, characterization of LCF behavior of SS 316 marks an important frontier for further investigation.

Martin-Meizoso et al. [4] conducted high-temperature LCF tests on 316 stainless steel at 600–625 °C. Despite the theoretical concerns about the applicability of J-integral to cyclic loading, as per their experience, they proposed a unique relationship, which existed for high- and low-cycle fatigue crack growth rates (and lives) when expressed in terms of J-integral. Fatemi and Yang [5] made a comprehensive review of the fatigue damage theories in the period of time commencing early 1970s to the early 1990s. All the theories were grouped under six categories namely, (a) linear damage rules, (b) non-linear damage curve, (c) life curve modification methods, (d) approaches based on crack growth concept, (e) continuum damage mechanics, and (f) energy based theories. Ganesh Sundara Raman and Radhakrishnan [6] used Manson–Coffin and Basquin relations in conjunction with the cyclic stress–strain curve in LCF of metallic materials. Based on the above relations, they discussed various design considerations under constant load range or constant total displacement range.

Thus, the present work is planned to characterize LCF behavior of SS 316 stainless steel. LCF experimentation and FE simulation are used together to calibrate and simulate the material under LCF test. Finite-element package ABAQUS is used for FE simulation in the elastic–plastic regime. Calibration and tuning of LCF parameters of the material SS 316, from experimental and FE simulated results for LCF behavior, is followed by damage calculations and life prediction in LCF loading.

Mathematical formulation

For finite-element simulation of LCF, the ABAQUS software is used. For the simulation of LCF in FE analysis, appropriate plastic modulus formulation along with modeling of hardening is necessary. There are several models available in ABAQUS for modeling plasticity and hardening (kinematic and isotropic both). In this work, plastic modulus formulation with Zeigler kinematic hardening rule [7] and exponential isotropic hardening rule have been used.

Plastic modulus formulation with Zeigler kinematic hardening rule and exponential isotropic hardening rule:

(a) *Yield function*: The yield function used in the current model is a von Mises yield function. With kinematic hardening, it is represented as follows:

$$f = \frac{3}{2}(S_{ij} - \alpha_{ij})(S_{ij} - \alpha_{ij}) - \sigma_{yc}^2 = 0 \quad (1)$$

S_{ij} denotes the deviatoric stress tensor, i.e.,

$$\sigma_{ij} = S_{ij} + \sigma_{\mathrm{m}}\delta_{ij} \quad (2)$$

α_{ij} and σ_{m} denote back stress tensor and the mean, stress respectively. σ_{yc} denotes the current yield stress.

(b) *Flow rule*: Associated flow rule is given by:

$$\mathrm{d}\bar{\varepsilon}^{\mathrm{p}} = \frac{1}{H}(\hat{n} \cdot \mathrm{d}\bar{\sigma})\hat{n} \quad (3)$$

where $\mathrm{d}\bar{\varepsilon}^{\mathrm{p}}$ denotes plastic strain rate vector. Here, H stands for plastic hardening modulus. $\mathrm{d}\bar{\sigma}$ denotes stress rate vector. $\hat{n}$ referred to as the flow vector, represents the unit normal to the yield surface, i.e.,

$$\hat{n} = \frac{\frac{\partial f}{\partial \bar{\sigma}}}{\left|\frac{\partial f}{\partial \bar{\sigma}}\right|}.$$

(c) *Hardening rule*: Change of the yield surface loci in stress space with increasing plastic strain is referred to as hardening. It can be classified into two types, isotropic hardening and kinematic hardening. There are different types of hardening laws that take into account the effect of kinematic hardening.

In this case, hardening rule employed is Zeigler kinematic hardening law. The kinematic hardening component is defined to be an additive combination of a purely kinematic term (linear Zeigler hardening law-accounting for the yield surface translation in deviatoric stress space) and a relaxation term (the recall term), which introduces the non-linearity. Another form of hardening is the isotropic hardening accounting for the expansion of the yield surface without its translation. The evolution of the deviatoric back stress, is represented mathematically as follows:

$$\dot{\bar{\alpha}} = C\frac{1}{\sigma_0}(\bar{S} - \bar{\alpha})\dot{\varepsilon}_{\mathrm{eq}}^{\mathrm{p}} - \gamma\bar{\alpha}\dot{\varepsilon}_{\mathrm{eq}}^{\mathrm{p}}. \quad (4)$$

Also, we have

$$\dot{\varepsilon}_{\mathrm{eq}}^{\mathrm{p}} = \left|\dot{\varepsilon}_{kl}^{\mathrm{p}}\right| = \left[\frac{2}{3}\dot{\varepsilon}_{ij}^{\mathrm{p}}\dot{\varepsilon}_{ij}^{\mathrm{p}}\right]^{\frac{1}{2}} = \lambda\left[\frac{2}{3}\frac{\partial f}{\partial \sigma_{ij}}\frac{\partial f}{\partial \sigma_{ij}}\right]^{\frac{1}{2}}. \quad (5)$$

The material parameters, C and γ are found out from the experimental stress–strain loop data [8].

For the isotropic hardening rule, Chaboche [9] proposed the following equation:

$$\dot{R}(\varepsilon_{\mathrm{eq}}^{\mathrm{p}}) = b(Q - R)\dot{\varepsilon}_{\mathrm{eq}}^{\mathrm{p}}, \quad (6)$$

where b and Q are the isotropic hardening material parameters and are computed from experimental stress–strain loop results of LCF test of plain fatigue specimens. Using the initial condition, i.e., $R(\varepsilon_{\mathrm{eq}}^{\mathrm{p}}) = 0$, on integration of the above differential equation, we get

$$R = Q\left(1 - e^{-b\cdot\varepsilon_{\mathrm{eq}}^{\mathrm{p}}}\right). \quad (7)$$

Fially, the elastic–plastic tensor, D_{ijkl}, is represented as

$$D_{ijkl} = E_{ijkl} - \frac{1}{H}E_{ijmn}\frac{\partial f}{\partial \sigma_{mn}}E_{klop}\frac{\partial f}{\partial \sigma_{op}}. \quad (8)$$

Here, E_{ijkl} is the fourth-order elastic tensor.

This material modeling for cyclic plasticity is available as "built-in-model" in ABAQUS and is used here to generate stress–strain results under strain-controlled cyclic loading. Necessary material properties required are measured from tensile and LCF tests and given as input and FE results are obtained from ABAQUS.

LCF experiments

The experimental LCF test was carried out under *strain-controlled loading* conditions in INSTRON UTM (Universal Testing Machine) with 8800 controller at room temperature for different strain amplitudes (0.30–1.20%). A dynamic extensometer of 12.5 gauge length is used. The strain rate is 0.001 s^{-1}. A triangular waveform is used for this test.

From Figs. 1, 2, and 3, the following inferences were drawn:

1. The hardening saturates after 30 cycles.
2. For, $\varepsilon_a = 0.3$–0.75% shows an initial hardening, a flat plateau for a large number of cycles and then softening before failure.

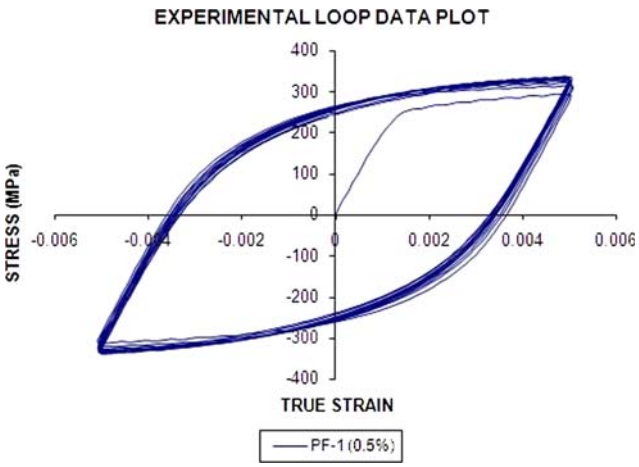

Fig. 1 Loop data plot (0.5% strain amplitude)

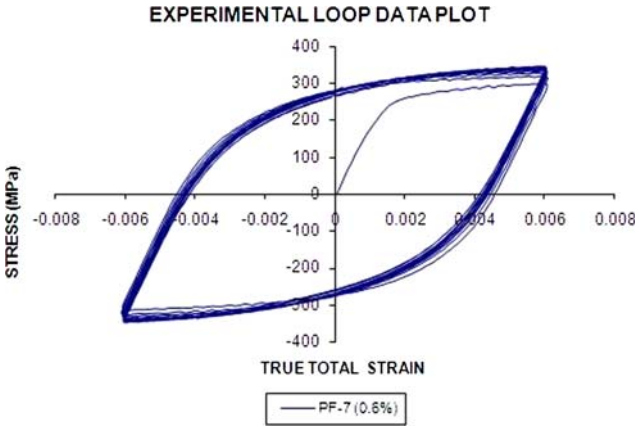

Fig. 2 Loop data plot (0.6% strain amplitude)

3. For, $\varepsilon_a = 1.0$ and 1.20% shows secondary hardening before failure. Also, it can be observed that the cyclic hardening rate increase with strain amplitude.

Finite-element simulation

The first 30 cycles of the LCF experiments have been simulated by elastic–plastic finite-element method in finite-element package ABAQUS (ABAQUS-6.7 finite-element software). The kinematic hardening coefficients are determined from experimental saturated loop data. Those values, along with other material properties are listed in Table 1.

Figure 4 shows a comparison between simulated and experimental saturated loop. The matching is satisfactory in the engineering sense. Some mismatches occur in loop data at the initial parts of loading and unloading branch.

Table 1 Material properties used in simulation

Material constants	Elastic properties	E: 200 GPa	
		υ: 0.3	
	Hardening properties	σ_0: 225 MPa	
		Kinematic hardening parameters (stabilized cycle)	C: 42096 MPa
			γ: 594.45
		Cyclic hardening parameters	b: 9.71
			Q_∞: 60 MPa

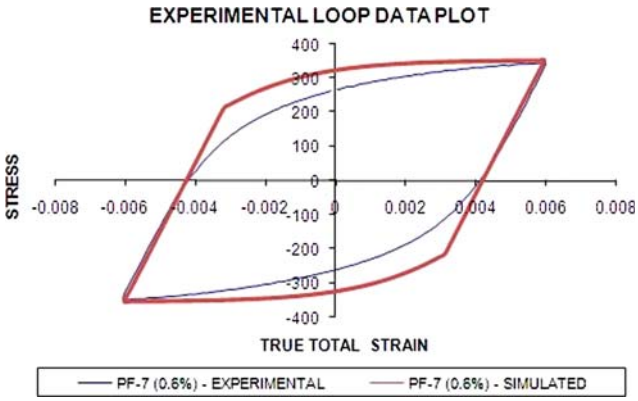

Fig. 4 Comparison of simulated saturated loop against saturated experimental loop (Cycle 30; 0.6%)

A single segmented kinematic hardening law (Zeigler kinematic hardening law) suffers from this discrepancy. A multi-segmented Chaboche's law [10] will yield better result. As the software ABAQUS is restricted only to Zeigler kinematic hardening model, we had to bear with this discrepancy.

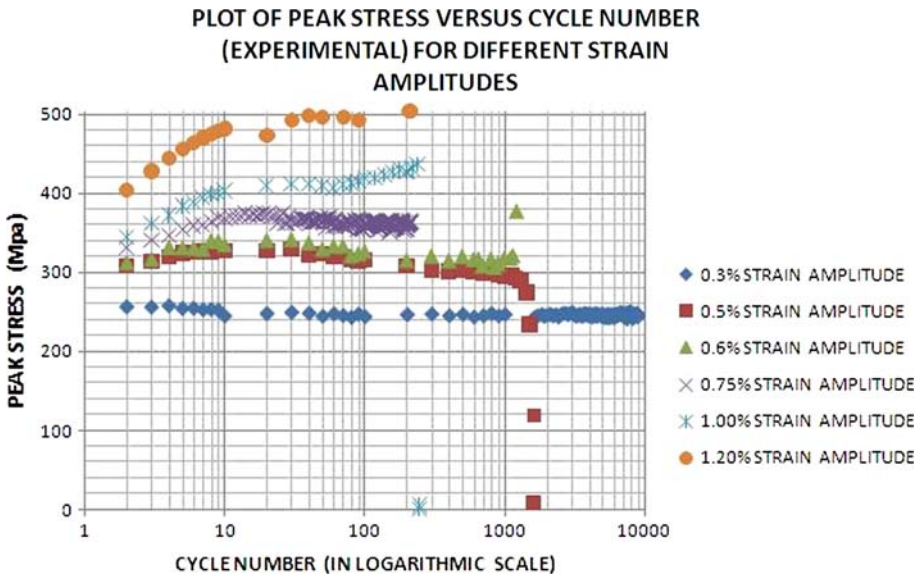

Fig. 3 Peak stress versus cycle number (experimental)

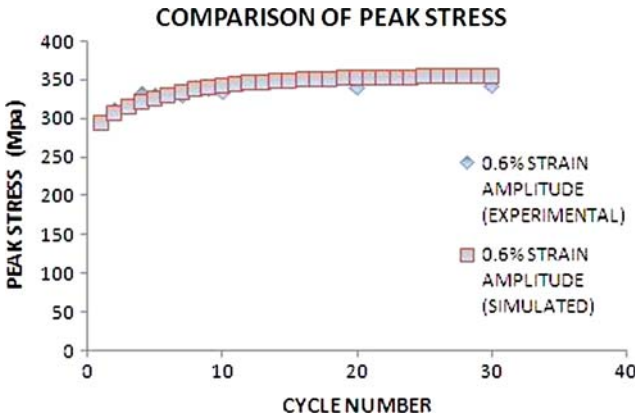

Fig. 5 Comparison of simulated peak stress against experiments (0.5%)

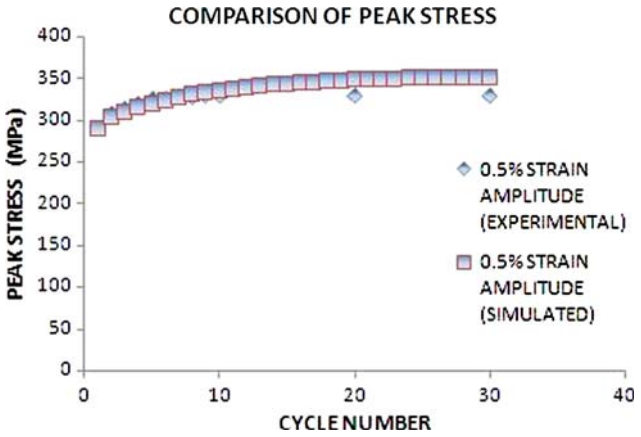

Fig. 6 Comparison of simulated peak stress against experiments (0.6%)

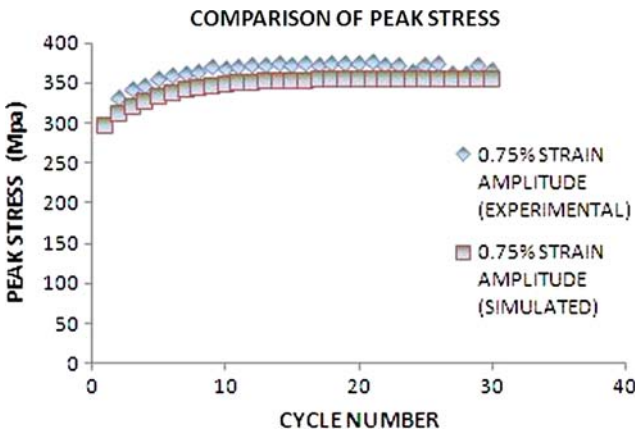

Fig. 7 Comparison of simulated peak stress against experiments (0.75%)

Figures 5, 6, and 7 show the comparison of peak stress variation with cycles. The simulated results show a good match with experimental results. The matching is acceptable in engineering sense.

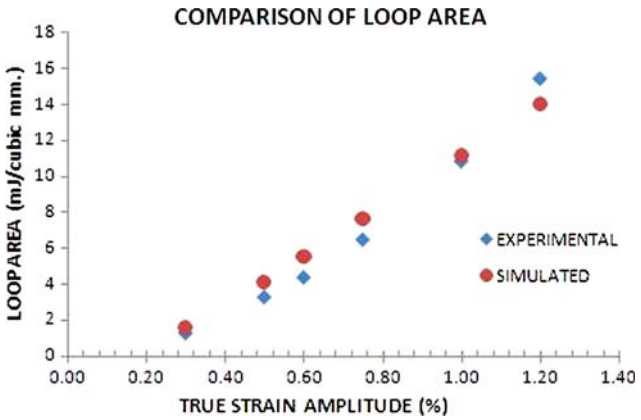

Fig. 8 Comparison of loop area

Fatigue damage and life prediction

The loop areas for simulated saturated loops are computed for various strain amplitude. These are compared with experimental values. Figure 8 shows such comparison. The matching is acceptable in engineering sense. Fatigue strain life is generated from the experimental results.

The usual way of representing low-cycle fatigue test results is to plot the plastic strain range $\Delta\varepsilon_p$ against N, where N represents the number of cycles to failure. This is plotted on log–log coordinates and this type of behavior is known as the *Coffin–Manson relation*, which is best described by:

$$\frac{\Delta\varepsilon_p}{2} = \varepsilon'_f(2N)^c \tag{9}$$

where, ε'_f is the *Fatigue Ductility coefficient*, c the *Fatigue ductility exponent*. The approach preferred here is to use the linear model for fitting linear range of the data. Figure 10 shows the fatigue strain life curve for the material SS 316. The fatigue ductility coefficient (ε'_f) is found out to be, $\varepsilon'_f = 0.0779834$ and, the fatigue ductility exponent (c) is found out to be, $c = -0.38479$.

LCF damage is estimated by Smith–Watson–Topper model, which is described by:

$$\sigma_{\max}\varepsilon_a = \sigma_{a,\mathrm{rev}}\varepsilon_{a,\mathrm{rev}} = \sigma'_f\varepsilon'_f(2N)^m. \tag{10}$$

In this model, the *fatigue strength limit*, σ'_f, is assumed to be equal to the true uniaxial fracture stress of the material, i.e., $\sigma'_f = 1177.609$ Mpa and, the value of *fatigue ductility coefficient*, ε'_f, is approximated to be equal to the uniaxial ductility (true fracture strain) of the material, i.e., $\varepsilon'_f = 0.53057$. SWT model is calculated from experimental as well as simulated results. It is found that the value of $m = -0.622290$ for the material SS 316.

Finally, the LCF damage is estimated from plastic strain energy dissipation per cycle (loop area). The coefficients

Table 2 Comparison of failure cycles

Strain amplitude (%)	Failure cycle			
	Experimental	Coffin–Manson relation	Smith–Watson–Topper	Plastic strain energy
0.30	8835	9219	7379	8057
0.50	1600	1689	1585	1577
0.60	1070	895	1050	856
0.75	216	447	590	440
1.00	212	192	305	194
1.20	209	121	211	125

"K" and "m" are also calculated from experimental as well as simulated results.

$$W_f = \Delta W N_f = K N_f^m \quad (11)$$

where, W_f is the total plastic strain energy dissipated prior to failure and, ΔW the average plastic strain energy dissipated per cycle. It is found that $m = 0.4809092$, and $K = 178.1085$ for the above criterion.

The fatigue life curves from all the three criteria are compared in Figs. 12 and 13. It is found that the life prediction for LCF is almost/identical for all these three criteria. Table 2 shows a comparison of actual life obtained from experiments and the predicted life from these criteria.

Discussion and conclusion

The present work is an attempt to calibrate the material SS 316 for low-cycle fatigue behavior. In order to pursue this work LCF, experiments have been done at different strain amplitudes (0.3–1.20%). Cyclic hardening is observed from the experimental loop curves which saturates after 30 cycles as is seen in Fig. 3. Most of the curves ($\varepsilon_a = 0.3$–0.75%) show initial hardening, a flat plateau for a large number of cycles and then softening before failure. Two curves ($\varepsilon_a = 1.0$ and 1.20%) show secondary hardening before failure. It is also observed that the cyclic hardening rate increases with strain amplitude.

The present work is to simulate the first 30 cycles of the LCF experiments by elastic–plastic finite-element method by using finite-element package, ABAQUS. The kinematic hardening coefficients are determined from experimental saturated loop data. The hardening is also calibrated to saturate after 30 cycles as was found in experimentation.

Comparison between simulated and experimental saturated loop is satisfactory in engineering sense, as is shown in Fig. 4. Figures 5, 6, and 7 show the comparison of peak stress variation, with cycles, both for simulated and experimental results wherein, a good match is observed for strain amplitude of 0.5 and 0.6%. In case of 0.75% strain amplitude, the variation between experimental results and simulated results is relatively large. This is due to two reasons. One, the values of kinematic hardening parameters (C and γ) have been extracted from the LCF data of 0.5% strain amplitude. Therefore, the variation between experimental results and simulated results may occur at higher strain amplitudes. The average values of C and γ computed from LCF data of all the strain amplitudes may smother the variation. Second, the yield stress obtained from cyclic loop data is observed to increase with strain amplitude but in this case the value of yield stress obtained from monotonic loading is used. This is the major cause of variation between experimental results and simulated results at higher strain amplitudes. The loop areas for simulated saturated loops are computed for various strain amplitudes. These are compared with experimental values. Figure 8 shows such a comparison. The matching is acceptable in engineering sense. The stress–strain curve for the saturated loop for different strain amplitudes are shown in Fig. 9. The cyclic stress–strain curve for this material is obtained by joining the peak values, which is also presented in Fig. 9.

Fatigue strain life curve is generated from the experimental results. Figure 10 shows the fatigue strain life curve for the material SS 316. The value of fatigue ductility coefficient (ε_f') is found out to be, $\varepsilon_f' = 0.0779834$ and, the value of fatigue ductility exponent (c) is found out to be, $c = -0.38479$. LCF damage is estimated by Smith–Watson–Topper model. In this model, the fatigue strength limit is assumed to be equal to the true uniaxial fracture stress of the material, i.e., $\sigma_f' = 1177.609$ Mpa and, the fatigue ductility coefficient is approximated to be equal to the uniaxial ductility (true fracture strain) of the material, i.e., $\varepsilon_f' = 0.53057$. SWT model coefficients are calculated from experimental as well as simulated results. It is found that the value of $m = -0.622290$ for the material SS 316. Finally, the LCF damage is estimated from plastic strain energy dissipation per cycle (loop area). The coefficients "K" and "m" are also calculated from experimental as well as simulated results. It is found that $m = 0.4809092$, and $K = 178.1085$ for the above criterion (Fig. 11).

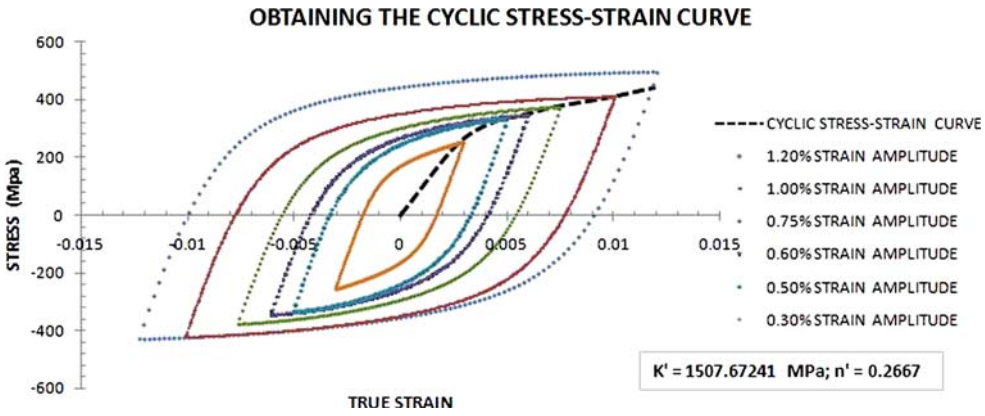

Fig. 9 Cyclic stress–strain curve

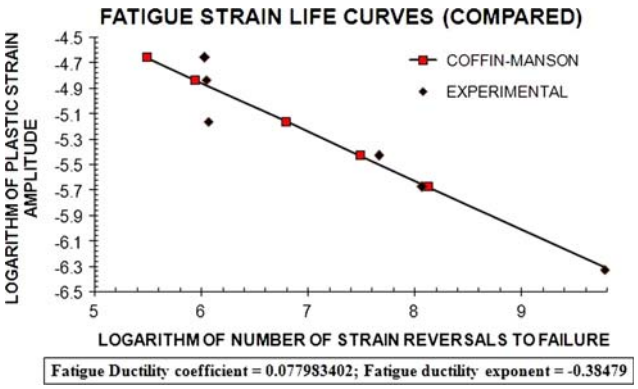

Fig. 10 Fatigue strain life curve (Coffin–Manson)

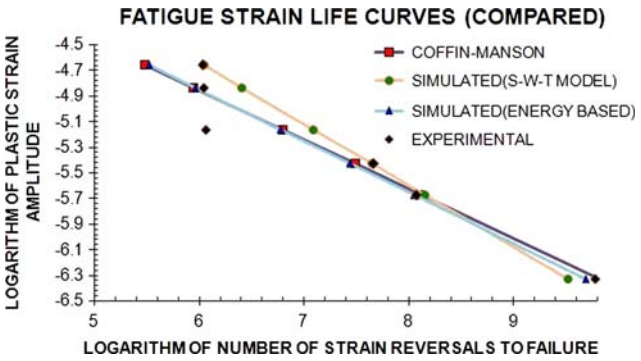

Fig. 12 All the three criteria's compared

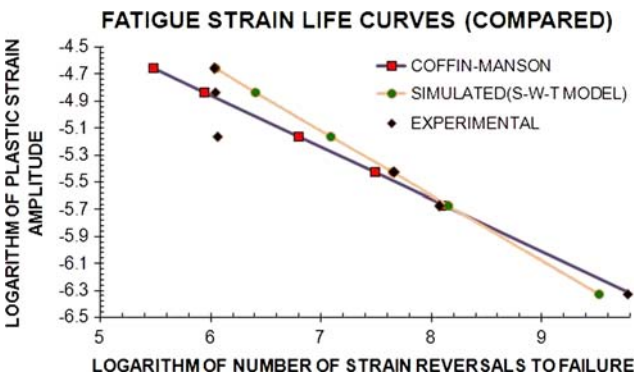

Fig. 11 Fatigue strain life curve (Coffin–Manson and Smith–Watson–Topper)

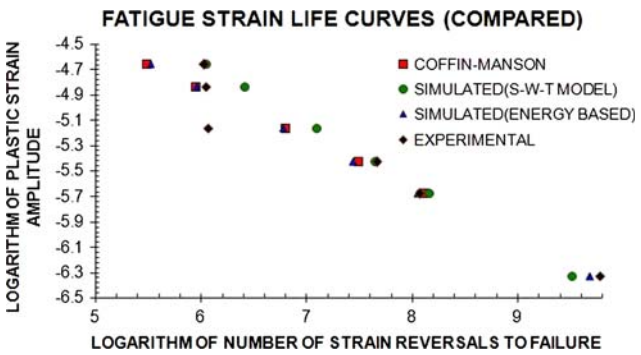

Fig. 13 Comparison of failure cycles

The fatigue life curves from all the three criteria are compared in Figs. 12 and 13. It is found that the life prediction for LCF is almost identical for all these three criteria. Table 2 shows a comparison of actual life obtained from experiments and the predicted life from these criteria.

From the above discussion, the following conclusions are drawn for LCF behavior of the material SS 316:

1. In LCF behavior, SS 316 shows cyclic hardening for first 30 cycles. The cyclic hardening gets saturated after 30 cycles.
2. Cyclic hardening rate increases with strain amplitudes.
3. At higher strain amplitudes ($\geq$1.00%) secondary hardening is observed. This may be due to change in micro-structure of the material in repeated load at higher plastic strain amplitude. Stainless steel (SS 316,

SS 304) has a tendency of formation of martensite at high plastic strain amplitude.

4. Zeigler non-linear kinematic hardening law simulates the saturated loop well in engineering sense. Better matching will be obtained with multi-segmented Chaboche's law. The work is in progress in this direction.
5. The loop area obtained from FE simulated saturated loop matches well with the experimental value and can be used for damage calculation in LCF loading of SS 316.
6. For life prediction in LCF of the material SS 316, all the three criteria namely,

   (i) Fatigue strain life curve (Coffin–Mansion)
   (ii) Smith–Watson–Topper model, and
   (iii) Plastic energy dissipation per cycle (loop area), predicts identical results.

References

1. Sandusky DW, Okada T, Saito T (1990) Mater Perform 29:66
2. Singh PK, Bhasin V, Vaze KK, Ghosh AK, Kushwaha HS (2008) Structural integrity of main heat transport system piping of AHWR. Health Safety and Environment Group, BARC, Mumbai, India
3. Wong YK, Hu XZ, Norton MP (2001) J Test Eval Am Soc Test Mater 29:138
4. Martin-Meizoso A, Rodriguez-Ibabe JM, Fuentes-Perez M (1993) Int J Fract 64:R45
5. Fatemi A, Yang L (1998) Int J Fatigue 20:9
6. Ganesh Sundara Raman S, Radhakrishnan VM (2002) Mater Des 23(3):249
7. Zeigler H (1959) Q Appl Mech 17:55
8. Chen WR, Keer LM (1991) An application of incremental plasticity theory to fatigue life prediction of steels. J Eng Mater Technol 113:404
9. Chaboche JL, Nouailhas D (1989) Trans ASME 111:384
10. Chaboche JL (1986) Int J Plast 2:149